Journal of Vibration and Acoustics. Received January 11, 2019;
Accepted manuscript posted March 13, 2019. doi:10.1115/1.4043241
Copyright © 2019 by ASME

Gain tuning for high speed vibration control of a multilink flexible manipulator using artificial neural network

Waweru Njeri*
Ph.D Student,
Department of Mechanical Engineering
Gifu University
1-1 Yanagido, Gifu, Japan
Email: v3812104@edu.gifu-u.ac.jp

Minoru Sasaki
Senior Professor, Fellow of ASME
Department of Mechanical Engineering
Gifu University
1-1 Yanagido, Gifu, Japan
Email: sasaki@gifu-u.ac.jp

Kojiro Matsushita
Associate Professor
Department of Mechanical Engineering
Gifu University
1-1 Yanagido, Gifu, Japan
Email: kojirom@gifu-u.ac.jp

ABSTRACT

Flexible manipulators are associated with merits like low power consumption, use of small actuators, high speed and their low cost due to fewer materials requirements than their rigid counterparts. However, they suffer from link vibration which hinders the aforementioned merits from being realized. The limitations of link vibrations are time wastage, poor precision and the possibility of failure due to vibration fatigue. This paper extends the vibration control mathematical foundation from a single link manipulator to a 3D, two links flexible manipulator.

*Address all correspondence related to this article to this author.

Journal of Vibration and Acoustics. Received January 11, 2019;
Accepted manuscript posted March 13, 2019. doi:10.1115/1.4043241

The vibration control theory developed earlier feeds back a fraction of the link root strain to increase the system damping, thereby reducing the strain. This extension is supported by experimental results. Further improvements are proposed by tuning the right proportion of root strain to feed back, and the timing using artificial neural networks. The algorithm was implemented online in Matlab interfaced with dSPACE for practical experiments. From the practical experiment, done in consideration of a variable load, Neural network tuned gains exhibited a better performance over those obtained using fixed feedback gains in terms of damping of both torsional and bending vibrations and tracking of joint angles.

Keywords*: Flexible manipulator, link vibrations, neural networks, strain feedback gain tuning*

1 Introduction

In the recent past, application of robots in manufacturing is on the rise showing up in areas previously thought infeasible like in soldering and in complex assembly tasks. The popular choice for applications such as the aforementioned is the flexible link manipulators owing to their low operation cost due to small actuators used, light weight and thus minimal inertia. The main limitation however, is that flexible robots are characterized by link vibrations, especially for high speed operations. The problem deteriorates with loading and additional joints and links. Link vibration far outweighs all the aforementioned merits associated with the flexible manipulator as it leads to time wastage, poor precision and can lead to mechanical failure as a result of vibration fatigue[1–7].

Luo in [8] proposed the Direct Strain Feedback(DSFB) and therein derived a mathematical proof that feeding a proportion of the link root strain increases system damping thereby enhancing vibration control of a one link flexible manipulator [9, 10]. The author also presented a rigorous proof of the stability of direct strain feedback control. Authors in [11] extended the concept earlier presented as a linear problem and approached it as a nonlinear problem, giving more insights in terms of control theory and stability of the scheme. The main strength of the direct strain feedback control is its simplicity in that the model of the plant is not required for controller design, only joint angles and root strain measurements are required. This simplifies the design in terms of circuitry and instrumentation. In the same respect, this control scheme is based on the infinite dimensional model, thus, it does not suffer from truncation spillovers[12].

The constant feedback gain control system is limited in that it leads to high noise feedback which is adversely superimposed on the joint trajectories. In addition, this control system poorly handle unpredictable parameters and uncertainties like changes in loading and trajectories. Ideally, feedback gains should be adapted to changes in strain and manipulator joint trajectories. Such works are reported in [13] where the strain feedback gains is adapted to the changing area under the strain

Journal of Vibration and Acoustics. Received January 11, 2019;
Accepted manuscript posted March 13, 2019. doi:10.1115/1.4043241

curve. Similarly, in [12], adaptive controller and automatic tuning of feedback gains is achieved based on the link potential and kinetic energies.

In this article, we show that feeding back a portion of the root strain can damp vibration in both the bending and torsional senses in a 3D, two-link flexible manipulator. Noting that though strain feedback is good for increasing system damping and thereby reducing link flexure, much of it can interfere with the desired accuracy. We further propose the use of Artificial neural networks(ANN) to tune the strain feedback gains on-line. Therefore, tradeoff has to be made between improvement of performance in terms of link vibration and the accuracy of the joint trajectories.

ANN is a powerful mathematical system that resembles in principle the working of the brain regarding learning, generalization, adaptation and the organization. Knowledge acquired by learning from its environment and the examples presented to it is stored as the experience in the inter-neuron connection weights. Learning is accomplished by presenting the network with input-output patterns, adjusting the weights based on the output error until a predetermined criterion is satisfied by using learning methods such as backpropagation algorithm. [14–17].

The backpropagation method is a gradient descent method that governs the evolution of interconnection weights in a multilayer neural network. During training, the input terminals are excited with a set of inputs signals which propagate forward, weighted by interconnection weights to yields the network output from the output layer. The resulting output of every neuron in the output layer is compared with the desired output for each unit, the error is backpropagated through the network in order to adjust the weights. This process repeats iteratively until the performance criterion is met[18–20].

The main contribution of this article is the mathematical demonstration that strain feedback increases damping of both bending and torsional vibration in a multi-link flexible manipulator and successful mathematical development of a backpropagation based neural network method that tunes the strain feedback gains of a two link 3D flexible manipulator. This results in a superior performance as compared to fixed feedback gains in terms of link strain and joint trajectories.

Vibration control is a subject receiving a lot of attention from researchers. Ripamonti et als in [21] recently reported vibration control method involving sliding mode control. In their work, the nonlinear model of a three-link flexible manipulator is obtained by system identification. Terminal sliding mode control is applied to the model resulting in considerable reduction in link vibrations. Other notable techniques reported in literature include μ-synthesis robust control[22, 23], vibration control based on internal resonance [24], input shaping[25] and boundary control with disturbance observers[26] to mention just but a few.

The rest of the paper is organized as follows. The 3D, two-link flexible manipulator is briefly introduced in section 2. The effect of strain feedback on the performance of the flexible manipulator system in abstract spaces is presented in

Journal of Vibration and Acoustics. Received January 11, 2019;
Accepted manuscript posted March 13, 2019. doi:10.1115/1.4043241

section 3. Gravity compensation due to self-weight of the links is highlighted in section 4. The neural network gain tuning problem formulation and experimental design is presented in section 5. Simulation and experimental results are presented and discussed in section 6 followed by conclusion in section 7.

2 Description of the Two link 3D flexible manipulator

The manipulator presented in this paper has two flexible links and it has a variable load at the distal end. It is sitting on a rotary joint giving the arrangement three degrees of freedom. Three dc servomotors drives the joints through servo amplifiers. The system is controlled from a personal computer running the MATLAB Simulink™ and interfaced with dSPACE™ applications. Speeds of the servomotors are reduced using harmonic drives having a drive ratio of 100 fitted between motor shafts and the joints.

Strain gauges are attached at the root of the links to capture bending and torsional flexure information which is conditioned using Wheatstone bridges before amplification using strain amplifiers for display. The control setup is as shown in Figure 1(See Table 1 in Appendix A.1 for specifications of the manipulator system).

3 Direct strain feedback system

This paper presents a 3D, two-link flexible manipulator having one end of each link $i(i = 1, 2)$ clamped to the control motor. The other end of each link has a variable tip body rigidly attached at the free end(For link 1, motor number 3 is regarded as a concentrated mass m_1). The flexible link i having length l_i, uniform linear mass density ρ_i per unit length, uniform flexural rigidity E_iI_i, uniform torsional rigidity G_iI_i and satisfies the Euler-Bernoulli hypothesis. The two-link system is sitting on a rotary joint driven by another control motor giving the manipulator system three degrees of freedom.

For simplicity, we assume that the joints are perfect and thus transverse vibrations and torsional vibrations are decoupled though transverse and torsional vibrations for links 1 and 2 are coupled. Hence, motion is governed by a pair of decoupled system of coupled partial differential equations with decoupled boundary conditions.

The main objective of this section is to show that both bending and torsional vibrations can be damped by feeding back a fraction of the respective root strains to the three respective control motors in generic abstract space.

Before the proof is given, a block diagram of the *dc* servomotor system for the joint drives upon which control of the manipulator is based on is presented.

Figure 2 is a block diagram of the dc servomotor system. In the model:

k - Strain feedback gain

k_0	-	Proportionality constant
k_1	-	Amplifier gain constant
k_2	-	Motor torque constant
k_3	-	Back emf constant
R_a	-	Armature winding resistance
L_a	-	Armature winding inductance
J_m	-	Inertia of the motor, load and the gear system referred to the motor shaft
b_m	-	Viscous friction coefficient of the motor, load and the gear system referred to the motor shaft
n	-	Harmonic drive ratio
θ_r	-	Joint reference angle
$\theta(t)$	-	Motor shaft angle
τ_m	-	Motor torque
τ_d	-	Disturbance torque
$\varepsilon(0,t)$	-	Root strain ($w''(0,t)$, $\phi'(0,t)$ for bending and torsion vibration respectively)

When the shaft is tracking the reference angle $i.e.\ \theta(t) \rightarrow \theta_r(t)$, the reference joint velocity:

$$\dot{\theta}_r = -k_0 k_1 k \varepsilon(0,t) \tag{1}$$

Neglecting armature inductance L_a, motor torque is given by

$$\tau_m(t) = \frac{1}{R_a}(\dot{\theta}_r - k_3\dot{\theta}(t)) \tag{2}$$

For small values of R_a

$$\dot{\theta}_r(t) = k_3\dot{\theta}(t) \tag{3}$$

also

$$\frac{J_m}{k_2}\ddot{\theta}(t) - \frac{b_m}{k_2}\dot{\theta}(t) = \tau_m(t) - \tau_d(t)$$

Journal of Vibration and Acoustics. Received January 11, 2019;
Accepted manuscript posted March 13, 2019. doi:10.1115/1.4043241

equating 1 and 3

$$
\begin{aligned}
k_3\dot{\theta}(t) &= -k_0 k_1 k \varepsilon(0,t) \\
\dot{\theta}(t) &= -\frac{k_0 k_1 k}{k_3}\varepsilon(0,t)
\end{aligned}
$$

without loss of generality, let $-\frac{k_0 k_1 k(t)}{k_3}$ be equal to unity and differentiating once $w.r.t$ time

$$\ddot{\theta}(t) = k\dot{\varepsilon}(0,t) \tag{4}$$

3.1 Torsional vibration

Now consider the manipulator in its vertical position, θ_2 =θ_3 = 0,(Refer to Figure 3), and joint number 1 is driven to angle θ_1. Assuming that torsional vibrations excited are of small amplitude and thus, we can ignore the coupling between the transverse and the torsional vibrations. Torsional vibration[27] excited are governed by the following equation of motion

$$
\begin{aligned}
&\ddot{\phi}_1(z_1,t) - 2\delta_1\frac{G_1 I_1}{\rho_1 I_{P1}}\dot{\phi}_1''(z_1,t) - \frac{G_1 I_1}{\rho_1 I_{P1}}\phi_1''(z_1,t) = -\frac{G_1 I_1}{\rho_1 I_{P1}}\ddot{\theta}_1(t) \\
&\ddot{\phi}_2(z_2,t) - 2\delta_2\frac{G_2 I_2}{\rho_2 I_{P2}}\dot{\phi}_2''(z_2,t) - \frac{G_2 I_{P2}}{\rho_2 I_2}\phi_2''(z_2,t) = \\
&\qquad -\frac{G_2 I_{P2}}{\rho_2 I_2}\left\{\ddot{\theta}_1(t) + \ddot{\phi}_1(l_1,t)\right\}
\end{aligned}
\tag{5}
$$

The boundary conditions at $z_1 = 0, l_1$; $z_2 = 0, l_2$ are

$$
\begin{aligned}
\phi_1(0,t) &= 0 \\
G_1 I_1 \phi_1''(0,t) &= \tau_{m1} \\
G_1 I_1 \phi_1''(l_1,t) &= -I_{P1}\ddot{\phi}_1(l_1,t) \\
\phi_2(0,t) &= \phi_1(l_1,t) \\
G_2 I_2 \phi_2''(l_2,t) &= -I_{P2}\ddot{\phi}_2(l_2,t)
\end{aligned}
$$

where δ_1, $\delta_2 > 0$, are damping terms introduced to factor in natural internal viscous damping of the links, assumed to be of the voigt type. We treat the system above in the form of an abstract second order evolution equation in an appropriate Hilbert space $\mathcal{H}_1$ with the inner product $\langle\cdot,\cdot\rangle$. Defining the operator A on $\mathcal{H}_1$ which is known to be self-adjoint and positive definite with a compact inverse as

$$D(A) = \{u = [u_1, u_2, u_3, u_4, u_5, u_6, u_7]^T | u_1 \in \mathcal{L}_2, u_2 \in \mathcal{L}_2,$$

Journal of Vibration and Acoustics. Received January 11, 2019;
Accepted manuscript posted March 13, 2019. doi:10.1115/1.4043241

$$u_1'' \in \mathcal{L}_2, u_2'' \in \mathcal{L}_2, u_3 = u_1(l_1), u_4 = u_2(l_2),$$

$$u_5 = u_1''(l_1), u_6 = u_2''(l_2), u_7 = u_2''(0), u_1(0) = 0\}$$

$$A \begin{bmatrix} u_1 \\ u_2 \end{bmatrix} = \begin{bmatrix} -\frac{G_1 I_1}{\rho I_1} u_1''(z_1) \\ -\frac{G_1 I_1}{\rho I_2} u_2''(z_2) \end{bmatrix} \forall u \in D(A)$$

also, from the motor dynamics, in particular, equation 4;

$$\begin{aligned} \dot{\theta}_1(t) &= k\varepsilon_1(0,t) \quad \text{for link 1} \\ \dot{\theta}_1(t) + \dot{\phi}_1(l_1,t) &= k\varepsilon_2(0,t) \quad \text{for link 2} \end{aligned}$$

At the same time, for torsion, strain $\varepsilon(0,t) = \phi'(0,t)$. Hence

$$\begin{aligned} \dot{\theta}_1(t) &= k\phi_1'(0,t) \\ \dot{\theta}_1(t) + \dot{\phi}_1(l_1,t) &= k\phi_2'(0,t) \end{aligned}$$

differentiating once more $w.r.t$ time and introducing

$$\Pi_* \begin{bmatrix} u_1 \\ u_2 \end{bmatrix} = \begin{bmatrix} u_1'(0) \\ u_2'(0) \end{bmatrix}, \forall u \in D(A)$$

Appropriate substitution into the system in 5 and rearranging yields

$$\begin{aligned} \ddot{\phi}_1(t) + (2\delta_2 + k\Pi_*)\dot{\phi}_1(t) + A\phi_1(t) = &\quad 0 \\ \ddot{\phi}_2(t) + (2\delta_2 + k\Pi_*)\dot{\phi}_2(t) + A\phi_2(t) = &\quad 0 \end{aligned} \tag{6}$$

3.2 Bending vibration

For bending vibration, let Jm_i, $\theta_i(t)$, τ_{mi} and $w_i(t, z_i)$ be the moment of inertia of the rotor of motor i, the angle of rotation of the arm i, the input torque for arm i and the transverse displacement of the arm i at the time t and at a spatial point z_i respectively. Neglecting the effect of self-weight due to gravity and assuming that bending deflections in both links are small, and proceeding as in [28], the equation of motion governing the bending motion of the arm is

$$\ddot{w}_1(z_1,t) + 2\delta_3 \frac{EI_1}{\rho_1} \dot{w}_1''''(z_1,t) + \frac{EI_1}{\rho_1} w_1''''(z_1,t) = -z_1\ddot{\theta}_2 \tag{7}$$

Journal of Vibration and Acoustics. Received January 11, 2019;
Accepted manuscript posted March 13, 2019. doi:10.1115/1.4043241

$$\ddot{w}_2(z_2,t) + 2\delta_4 \frac{EI_2}{\rho_2}\dot{w}_2''''(z_2,t) + \frac{EI_2}{\rho_2} w_2''''(z_2,t) =$$
$$- z_2 \left\{ \ddot{\theta}_2(t) + \ddot{\theta}_3(t) + \ddot{w}_{1,l}'(t) \right\}$$
$$- \{l_1\theta_1(t) + \ddot{w}_{1,l}(t)\}\cos\theta_{2d} \tag{8}$$

and

$$w_1(0,t) = 0, w_1'(0,t) = \theta_1(t),$$
$$EI_1 w_1''(l_1,t) = EI_2 w_2''(0,t)$$
$$M\{l_1\theta_1(t) + \ddot{w}_1(l_1,t)\} + EI_2 w_2'''(0,t)\cos\theta_{2d} = EI_1 w_1'''(l_1,t)$$
$$w_2(0,t) = w_2''(l_2,t) = 0, w_2'(0,t) = \theta_2(t) + w_1'(l_1,t)$$
$$m_2\left[\ddot{w}_2(l_2,t) + l_2\left\{\ddot{\theta}_1 + \ddot{\theta}_2 + \ddot{w}_1'(l_1,t)\right\}\right]$$
$$+ m_2\left\{l_1\ddot{\theta}_1(t) + \ddot{w}_1(l_1,t)\right\}\cos^2\theta_{2d} = EI_2 w_2'''(l_2,t)$$
$$\tau_{m2} = J_1\theta_2 - EI_1 w_{1,0}''(t) \tag{9}$$
$$\tau_{m3} = J_2\theta_3 - EI_2 w_{2,0}''(t) \tag{10}$$

where

$$M = m_1 + (\rho_2 l_2 + m_2)sin^2\theta_{2d}$$

and δ_3, $\delta_4 > 0$ are damping terms introduced to factor in natural internal viscous damping of the links, assumed to be of the voigt type.

We treat equations above in a form of an abstract second order evolution equation in an appropriate Hilbert space $\mathcal{H}_2$, with inner product $\langle\cdot,\cdot\rangle$ and the induced norm $\|\cdot\|$. Also introducing an operator A on $\mathcal{H}_2$ as

$$D(A) =\{u = [u_1, u_2, u_3, u_4, u_5, u_6, u_7, u_8, u_9, u_{10}, u_{11},$$
$$u_{12}, u_{13}, u_{14}, u_{15}]^T | u_1 \in \mathcal{L}_2, u_2 \in \mathcal{L}_2, u_1'' \in \mathcal{L}_2,$$
$$u_2'' \in \mathcal{L}_2, u_3 = u_1(l_1), u_4 = u_2(l_2), u_5 = u_1'(l_1),$$
$$u_6 = u_2'(l_2), u_7 = u_1''(l_1), u_8 = u_2''(l_2),$$
$$u_9 = u_1'''(l_1), u_{10} = u_2'''(l_2), u_{11} = u_2(0),$$

Journal of Vibration and Acoustics. Received January 11, 2019;
Accepted manuscript posted March 13, 2019. doi:10.1115/1.4043241

$$u_{12} = u_1'(0), u_{13} = u_2'(0), u_{14} = u_1''(0),$$

$$u_{15} = u_2''(0)\}$$

$$A \begin{bmatrix} u_1 \\ u_2 \end{bmatrix} = \begin{bmatrix} -\frac{EI_1}{\rho_1} u_1''''(z_1) \\ -\frac{EI_2}{\rho_2} u_2''''(z_2) \end{bmatrix} \forall u \in D(A) \tag{11}$$

which is known to be self-adjoint and positive definite with a compact inverse. Together with equation 4 where for bending vibration

$$\begin{aligned} k\dot{w}_1''(z_1,t) =& \ddot{\theta}_2 \\ k\dot{w}_2''(z_2,t) =& \ddot{\theta}_2(t) + \ddot{\theta}_3(t) + \ddot{w}_{1,l}'(t) \\ & - \frac{1}{z_2}\{l_1\theta_1(t) + \ddot{w}_{1,l}(t)\}\cos\theta_{2d} \end{aligned}$$

Introducing

$$\Pi_* \begin{bmatrix} u_1 \\ u_2 \end{bmatrix} = \begin{bmatrix} u_1''(0) \\ u_2''(0) \end{bmatrix}, \forall u \in D(A) \tag{12}$$

Using the operators A and Π_* in 11 and 12, evolution equations 7 and 8 can be expressed as

$$\begin{aligned} \ddot{w}_1(t) + (2\delta_3 + k\Pi_*)\dot{w}_1(t) + Aw_1(t) = 0 \\ \ddot{w}_2(t) + (2\delta_4 + k\Pi_*)\dot{w}_2(t) + Aw_2(t) = 0 \end{aligned} \tag{13}$$

Looking closely at the system of equations 6 and 13 representing closed loop strain feedback systems through controller gain k, the following remarks can be made:

Remark 1. *Torsional and bending Strain feedback when effected as a negative feedback acts to increase system damping of bending and torsional vibration in a 3D, two-link flexible manipulator system.*

Remark 2. *Strain feedback does not affect the stiffness of the resulting system. This means that the vibration frequency is not affected by the provision.*

4 Gravity compensation system

In the instances when the manipulator is not in its vertical position, each link maintains a tilted state, so the arm is affected by gravity. As a result, the value of the bending strain does not converge to zero but remains to be a value of the

Journal of Vibration and Acoustics. Received January 11, 2019;
Accepted manuscript posted March 13, 2019. doi:10.1115/1.4043241

distortion caused by the self-weight of the links shown in Figure 4.

The bending moment which bears this offset in strain is dependent on the weight of the links w_1, w_3, the weight of joint 2, w_2, the weight attached at the end of link 2, w_4 and their horizontal distance from the vertical position. To fully study the adaptation scheme, the influence of the gravity on the strain must be considered and appropriately corrected.

To solve this problem, we introduced an equation that predicts and corrects this distortion caused by gravity from the joint angles. This equation is expressed as

$$\xi_1 = \alpha_1 \sin\theta_2 + \beta_1 \sin(\theta_2 + \theta_3) + \text{offset}_1$$

$$\xi_2 = \beta_2 \sin(\theta_2 + \theta_3) + \text{offset}_2$$

where the variables ξ_1 and ξ_2 are the corrections applied to the strain information for links 1 and 2 for them to have zero average. For this series of experiments, the coefficients were taken as α_1 = 0.06, β_1 = 0.06, β_2 = 0.0362, offset$_1$ = 0, offset$_2$ = 0.1.

5 Neural network gain tuning

From the previous discussion, we have seen that feeding back a fraction of the root strain can damp link vibration in a 3D, two-link flexible manipulator. We further propose a tuning technique that will further improve damping over the conventional fixed feedback gains. To that end, we propose to tune the gains using artificial neural network.

5.1 Multilayer neural network

A typical 2 layer neural network as the one shown in Figure 5, consists of an input port, an output layer and a hidden layer situated between the input port and the output layer. The network is excited with input vector **x** = $\{x_1, x_2, \cdots, x_{N_i}\}$ to yield vectors **h** = $\{h_1, h_2, \cdots, h_{N_h}\}$ and **y** = $\{y_1, y_2, \cdots, y_{N_o}\}$ in the hidden and output layers respectively. N_i, N_h and N_o denotes the number of inputs, number of neurons in the hidden and the output layers respectively.

For the feedforward path from the input to the hidden layer, each of the N_i inputs x_i, $i = 1, 2, \cdots, N_i$ is connected to the j_{th} hidden neuron's input through the weight v_{ji}, $j = 1, 2, \cdots, N_h$. Each of this neurons has a summer that accumulates all the weighted inputs to form a scalar quantity

$$\begin{aligned} z_j &= \sum_{i=1}^{N_i} v_{ji} x_i + v_{j0} x_0 \\ &= \sum_{i=0}^{N_i} v_{ji} x_i \end{aligned} \tag{14}$$

Journal of Vibration and Acoustics. Received January 11, 2019;
Accepted manuscript posted March 13, 2019. doi:10.1115/1.4043241

The neuron also has an activation function $\sigma_1(\cdot)$ which squashes this scalar sum to form the output of the hidden neuron *j* as

$$h_j = \sigma_1 \left\{ \sum_{i=0}^{N_i} v_{ji} x_i \right\}$$

Outputs of individual neurons in the hidden layer h_j, $(j = 1, \cdots, N_h)$ forms an output vector $\mathbf{h} = [h_1, \cdots, h_j, \cdots, h_{Nh}]^T$ expressed as

$$\mathbf{h} = \sigma_1 \left\{ \mathbf{V}^T \mathbf{x} \right\}$$

where **V** is an $N_h \times N_i$ interconnection weights matrix between the input port and the hidden layer and **x** is the input vector. In particular

$$\mathbf{V} = \begin{bmatrix} v_{11} & \cdots & v_{1i} & \cdots & v_{1N_i} \\ \vdots & \ddots & \vdots & \ddots & \vdots \\ v_{j1} & \cdots & v_{ji} & \cdots & v_{jN_i} \\ \vdots & \ddots & \vdots & \ddots & \vdots \\ v_{N_h 1} & \cdots & v_{N_h i} & \cdots & v_{N_h N_i} \end{bmatrix}$$

Similarly, from the hidden to the output layer, the output of the j_{th} neuron in the hidden layer, h_j is weighted with weight w_{kj}, $k = 1, 2, \cdots, N_o$ before being terminated to the k_{th} neuron in the output layer. This neuron having a summer yields a scalar quantity

$$\begin{aligned} z_k &= \sum_{j=1}^{N_h} w_{kj} h_j + w_{k0} h_0 \\ &= \sum_{j=0}^{N_h} w_{kj} h_j \end{aligned} \tag{15}$$

which is in turn squashed by the activation function $\sigma_2(\cdot)$ to yield the network output

$$y_k = \sigma_2 \left\{ \sum_{j=1}^{N_h} w_{kj} h_j \right\}$$

Gathering outputs $y_k(k = 1, \cdots, N_o)$ forms the output vector $\mathbf{y} = [y_1, \cdots, y_k, \cdots, y_{N_o}]^T$ expressed as

$$\mathbf{y} = \sigma_2 \left\{ \mathbf{W}^T \mathbf{h} \right\}$$

Journal of Vibration and Acoustics. Received January 11, 2019;
Accepted manuscript posted March 13, 2019. doi:10.1115/1.4043241

where **W** is an $N_o \times N_h$ weighting matrix interconnecting outputs of the hidden layer to the output layer and expressed as

$$\mathbf{W} = \begin{bmatrix} w_{11} & \cdots & w_{1j} & \cdots & w_{1N_h} \\ \vdots & \ddots & \vdots & \ddots & \vdots \\ w_{k1} & \cdots & w_{kj} & \cdots & w_{kN_h} \\ \vdots & \ddots & \vdots & \ddots & \vdots \\ w_{N_o1} & \cdots & w_{N_oj} & \cdots & w_{N_oN_h} \end{bmatrix}$$

5.2 Learning Algorithm

In this subsection, we present the backpropagation algorithm which describes how individual interconnection weights v_{ji} between input node i and neuron j in the hidden layer and w_{kj} connecting the output of neuron j in the hidden layer to the input of neuron k in the output layer are updated and upon which this work is based. To that end, consider a typical two layer neural network configured as in Figure 5, having N_i input nodes, N_h neurons in the hidden layer and N_o in the output layer. For neuron k in the output layer, we choose a cost function J defined as the square of the error between the output y_k and the desired output for that specific neuron y_d

$$J = \frac{1}{2}(y_d(n) - y_k(n))^2 = \frac{1}{2}e(n)^2$$

Inter-layer weights are updated using gradient descent as

$$v_{ji}(n+1) = v_{ji}(n) + \eta\frac{\partial J}{\partial v_{ji}} \tag{16a}$$

$$w_{kj}(n+1) = w_{kj}(n) + \eta\frac{\partial J}{\partial w_{kj}} \tag{16b}$$

where η is learning rate, v_{ji} and w_{kj} are the interconnection weights in the hidden and the output layers respectively(See Figure 5). Using the chain rule

$$\begin{aligned} \frac{\partial J}{\partial w_{kj}} &= \frac{\partial}{\partial w_{kj}}\left\{\frac{1}{2}\sum_{k=1}^{N_o} e(n)^2\right\} \\ &= e(n)\frac{\partial}{\partial w_{kj}}(y_d - y_k) \\ &= -e(n)\frac{\partial y_k}{\partial w_{kj}} \\ &= -e(n)\frac{\partial \sigma_2(z_k)}{\partial w_{kj}} \\ &= -e(n)\frac{\partial \sigma_2(z_k)}{\partial z_k}\frac{\partial z_k}{\partial w_{kj}} \end{aligned}$$

Journal of Vibration and Acoustics. Received January 11, 2019;
Accepted manuscript posted March 13, 2019. doi:10.1115/1.4043241

$$= -e(n)\frac{\partial \sigma_2(z_k)}{\partial z_k}h_j \tag{17}$$

defining the error function δ_k as

$$\delta_k = -e(n)\frac{\partial \sigma_2(z_k)}{\partial z_k}$$

equation 17 can be expressed as

$$\frac{\partial J}{\partial w_{kj}} = \delta_k h_j \tag{18}$$

For the hidden layer, the output of each neuron in the hidden layer contributes to the network output and therefore the error of each neuron in the output layer. Thus, in calculating the contribution of the interconnection weights v_{ji} to the performance index J, we have to sum all errors over $k = 1, \cdots, N_o$ as

$$\begin{aligned}
\frac{\partial J}{\partial v_{ji}} &= \frac{\partial}{\partial v_{ji}}\left\{\frac{1}{2}\sum_{k=1}^{N_o} e(n)^2\right\} \\
&= -\sum_{k=1}^{N_o} e(n)\frac{\partial y_k}{\partial v_{ji}} \\
&= -\sum_{k=1}^{N_o} e(n)\frac{\partial \sigma_2(z_k)}{\partial v_{ji}} \\
&= -\sum_{k=1}^{N_o} e(n)\frac{\partial \sigma_2(z_k)}{\partial z_k}\frac{\partial z_k}{\partial v_{ji}}
\end{aligned} \tag{19}$$

from equation 14 and 15

$$\begin{aligned}
z_k &= \sum_{k=1}^{N_o} w_{kj}h_j + w_{kj}h_0 \\
&= \sum_{k=1}^{N_o} w_{kj}\sigma_1(z_j) + w_{kj}h_0 \\
&= \sum_{k=1}^{N_o} w_{kj}\sigma_1\left\{\sum_j v_{ji}x_i + v_{j0}x_0\right\} + w_{kj}h_0
\end{aligned}$$

using chain rule and appropriate substitution yields

$$\begin{aligned}
\frac{\partial z_k}{\partial v_{ji}} &= \frac{\partial z_k}{\partial h_j}\frac{\partial h_j}{\partial v_{ji}} \\
&= \frac{\partial w_{kj}h_j}{\partial h_j}\frac{\partial h_j}{\partial v_{ji}}
\end{aligned}$$

Journal of Vibration and Acoustics. Received January 11, 2019;
Accepted manuscript posted March 13, 2019. doi:10.1115/1.4043241

$$
\begin{aligned}
&= w_{kj}\frac{\partial h_j}{\partial v_{ji}} \\
&= w_{kj}\frac{\partial \sigma_1(z_j)}{\partial v_{ji}} \\
&= w_{kj}\frac{\partial \sigma_1(z_j)}{\partial z_j}\frac{\partial z_j}{\partial v_{ji}} \\
&= w_{kj}\frac{\partial \sigma_1(z_j)}{\partial z_j}\frac{\partial}{\partial v_{ji}}(\sum_j v_{ji}x_i + w_{j0}x_0) \\
&= w_{kj}\frac{\partial \sigma_1(z_j)}{z_j}x_i \qquad (20)
\end{aligned}
$$

substituting 20 into 19, the update equation for the hidden layer as

$$
\begin{aligned}
\frac{\partial J}{\partial v_{ji}} &= -\sum_k e(n)\frac{\partial \sigma_2(z_k)}{\partial z_k}w_{kj}\frac{\partial \sigma_1(z_j)}{\partial z_j}x_i \\
&= -\frac{\partial \sigma_1(z_j)}{\partial z_j}x_i\sum_{k=1}^{N_o} e(n)\frac{\partial \sigma_2(z_k)}{\partial z_k}w_{kj} \\
&= -x_i\frac{\partial \sigma_1(z_j)}{\partial z_j}\sum_{k=1}^{N_o}\delta_k w_{kj} \\
&= \delta_j x_i \qquad (21)
\end{aligned}
$$

where

$$\delta_j = -\frac{\partial \sigma_1(z_j)}{\partial z_j}\sum_{k=1}^{N_o}\delta_k w_{kj}$$

Substituting equations 18 and 21 back to 16a and 16b and introducing momentum terms to enhance training, the weights in the two layers are to be updated as

$$v_{ji}(n+1) = v_{ji}(n) + \eta\delta_j x_i + \alpha\Delta v_{ji}(n) \qquad (22a)$$

$$w_{kj}(n+1) = w_{kj}(n) + \eta\delta_k h_j + \alpha\Delta w_{kj}(n) \qquad (22b)$$

where η and α are the learning and the momentum rates respectively. Detailed formulation of the learning process for gain tuning is presented in the following subsection.

5.3 Gain tuning problem formulation

The self-tuning strain feedback gain system configuration for each of the three control motors is as shown in Figure 6. The control law is derived from the joint angle error and the link strain pre-multiplied by the feedback gain k as

$$u_i(t) = \theta_{ri}(n) - \theta_i(n) - k_i\varepsilon_i(0,n) \quad \text{for } i = 1, 2, 3$$

Journal of Vibration and Acoustics. Received January 11, 2019;
Accepted manuscript posted March 13, 2019. doi:10.1115/1.4043241

where θ_{ri} is the desired joint trajectory, θ_i is the actual joint trajectory, $\varepsilon_i(0,n)$, $\varepsilon_i(0,n)$ is the sampled strain at root of the links and k_i is the feedback gain adaptively trained using an online neural network. Tansig activation function was employed in the hidden layer and linear function in the output layer.

Defining the performance index as a function of the root strain $\varepsilon_i(0,n)$

$$J \triangleq \frac{a}{2}\varepsilon_i(0,n)^2 \quad a \in \mathbb{R}^+ \tag{23}$$

Based on the steepest descent algorithm at the output layer

$$w_{kj}(n+1) = w_{kj}(n) + \eta\frac{\partial J}{\partial w_{kj}}$$

where

$$\begin{aligned}\frac{\partial J}{\partial w_{kj}} &= \frac{\partial J}{\partial \varepsilon_i(0,n)}\frac{\partial \varepsilon_i(0,n)}{\partial u(n)}\frac{\partial u(n)}{k\varepsilon_i(0,n)}\frac{\partial k(n)\varepsilon(0,n)}{\partial k(n)}\frac{\partial k(n)}{\partial z_k}\frac{\partial z_k}{\partial w_{kj}}\\ &= a\varepsilon_i(0,n)^2\frac{\partial \varepsilon(0,n)}{\partial u(n)}h_j\\ &= \delta_k h_j\end{aligned}$$

where

$$\delta_k = a\varepsilon_i(0,n)^2\frac{\partial \varepsilon(0,n)}{\partial u(n)} \tag{24}$$

considering the nonlinear nature of the plant, it is difficult to analytically determine the jacobian $\frac{\partial \varepsilon_i(0,n)}{\partial u(n)}$ in equation 24. To simplify the control system, we make the following assumption

Assumption 1. *The jacobian in equations 24 is equal to unity and both the sign and magnitude are compensated for by tuning the convergence factor.*

For the hidden layer having tansig activation function we have

$$\begin{aligned}\frac{\partial J}{\partial v_{ji}} &= \sum_{k=1}^{N_o}\frac{\partial J}{\partial z_k}\frac{\partial z_k}{\partial v_{kj}}\frac{\partial z_k}{\partial h_j}\frac{\partial h_j}{\partial z_j}\frac{\partial z_j}{\partial v_{ji}}\\ &= -\sum_{k=1}^{N_o}\delta_k w_{kj}\frac{\partial \sigma_1(z_j)}{\partial z_j}x_i\\ &= -\sum_{k=1}^{N_o}\delta_k w_{kj}(1-h_j^2)x_i\end{aligned}$$

Journal of Vibration and Acoustics. Received January 11, 2019;
Accepted manuscript posted March 13, 2019. doi:10.1115/1.4043241

$$= \delta_j x_i$$

where

$$\delta_j = -\sum_{k=1}^{N_o} \delta_k w_{kj}(1 - h_j^2) \tag{25}$$

Equations 24 and 25 are substituted back to equation 22 to complete weight update formulation.

6 Results and Discussion

6.1 Simulation results

Development of the strain feedback gain tuning system was initially simulated in Simulink. To this end, the dynamic model of flexible manipulator was modeled in Maple/Maplesim and extracted to Matlab using Maplesim/Matlab connector followed by validation against the actual manipulator. Simulink block to implement neural network gain tuner was developed as an $s - function$ coded in $c - language$.

Figure 7 shows the control law, link strain and the tuned gains obtained by employing the performance index defined in equation 23. In Figure 7c, it can be observed that the gains grow from an initial value when the link strain is not zero. However, when the strain reduce to negligible values owing to design and the natural damping, gains neither grow nor decay but remain constant only to grow again when strain changes. This is attributed to the fact that the gains are the area under the cost function J.

It is desired to have the gains grow to counter the link strain and decay to minimal values when the performance index reduce to a present value. To achieve this, the performance index was modified as follows

$$J = \begin{cases} \frac{a}{2}\varepsilon_i(0,n)^2, & \text{if } J \geq J_s \quad a \in \mathbb{R}^+ \\ -\frac{b}{2}k(n), & \text{if } J < J_s. \quad b \in \mathbb{R}^+ \end{cases}$$

where the modification is introduced to ensure that the gains reduce to a certain level awaiting to grow again when the performance index fall behind a certain threshold J_s. The variable b determines the rate of decay. Figure 8 shows the gains after the introduction of the modification term.

Comparison of the torsional and link strain is presented in Figure 9 considering the simulation performance with and without tuned strain feedback. From the figures, a significant reduction in strain is observed.

Journal of Vibration and Acoustics. Received January 11, 2019;
Accepted manuscript posted March 13, 2019. doi:10.1115/1.4043241

6.2 Experimental Results

The neural network configuration presented in this report has 6 inputs, 12 hidden neurons and 1 output neuron corresponding to the strain feedback gain k. The inputs to the network are $\theta(t)$, $e(t)$, $\varepsilon(0,t)$, $\theta(t-1)$, $e(t-1)$, $\varepsilon(0,t-1)$. In this experiment, a and b were set as (3000,0.8),(600,1),(600,1) for joints 1, 2 and 3 respectively, learning rate η = 2×10^{-4} and the sampling rate of 0.002. The experiment involved moving the three joints at an angle of 20 degrees using a step signal lasting for 10 seconds followed by returning the links to their original position for 10 more seconds.

Following results were obtained considering unloaded manipulator and one with a load of $100g$ attached at the distal end of link 2.

6.2.1 Without any load

Figure 10 show the link strain for the manipulator with neural network tuning and fixed gain $k = 0.5$. In the first 10 seconds when the manipulator is not in its vertical position, bending strain in both links does not converge to zero because of the self weight effect due to gravity. From the figure, we see that strain resulting from fixed gain was more severe than those resulting from tuned gains. This was largely attributed to enhanced damping due to a relatively higher tuned gain. To a lesser extent, when the motors stop, the encoder noise was fed back, minimal effects of this noise were experienced with the tuned gain where the gain was smaller as compared to the control system having fixed gain of 0.5.

Figure 11 show the joint trajectories for the manipulator with neural network tuning and fixed gain $k = 0.5$. Zooming into a region between 11-14 seconds of the joint 1 trajectory, we can see the adverse effect of constant gains on the joint trajectories. This is due to the fact that residual strain affect the control law which in turn affect the joint angles.

Figure 12 show the feedback gains for the manipulator with neural network tuning and fixed gain $k = 0.5$. The tuned gains can be seen rising from an initial value to counter link strain. When the strain reduces to a certain values dictated by the performance index J, the gains decays and remain minimal awaiting to grow again to counter future increase in strain. Minimal values of feedback gains has the strength of ensuring minimal strain gauge noise feedback.

To further appreciate the improvement in vibration control, Figure 13 show the strain power spectrum for the manipulator with neural network tuning and fixed gain.

6.2.2 With a load of 100g

To investigate the behavior of the arm when subjected to loading, experiments were further carried out with a load of 100g now attached at the distal end of link 2. Figure 14 show the link strain for the manipulator with neural network tuning and fixed gain. It can be observed that strain with loading are severe relative to the case when the arm is not loaded.

Journal of Vibration and Acoustics. Received January 11, 2019;
Accepted manuscript posted March 13, 2019. doi:10.1115/1.4043241

Figure 15 show the joint trajectories for the manipulator with neural network tuning and fixed gain. Again, region between 11-14 seconds has been zoomed in to show the effect of the two schemes on the joint trajectories. From the figure, we can see the gain tuning least adversely affect the joint trajectories.

Figure 16 show the feedback gains for the manipulator with neural network tuning and fixed gain. Like in the case without loading, the gains grow from an initial value to counter the strain only to decay after the performance index reaches a certain preset value. It can be noted that the gains in this case are relatively higher owing to the changes in loading which in turn leads to an increase in strength of strain.

Figure 17 show the strain power spectrum of the manipulator with neural network tuning and fixed gain with a load of 100g. The power is relatively higher than in the case without load and the superiority of self-tuning in performance is very evident. We can also observe that the natural frequencies in the loaded case are lower than those observed in the case without any load attached at the distal end of link number 2.

7 Conclusion

This paper presented a self-tuning strain feedback gain controller for a 3D, two-link flexible manipulator using artificial neural network for high speed control. The algorithm successfully learnt the suitable gain for the flexible manipulator, raising the gains in the instances when vibrations are severe followed by decay in gains to limit feedback noise when vibrations subsides. The results show that tuned gains achieves better performance than that achieved using fixed gain in terms of link strain and joint trajectories. This is attributed to the fact that though strain feedback increases system damping which reduces vibrations, it is only required when motors are in motion, when not in motion, it provides a feedback path for noise from the strain gauges. This adversely affect joint trajectories and it becomes worse with increased loading. Tuned gains on the other hands increase system damping when it is needed to counter link strain followed by lowering of gains to limit feedback noise. Thus, it provides a balance between vibration control and feedback noise attenuation.

8 Acknowledgement

This work is partially supported by grants-in-aid for promotion of Regional Industry-University-Government collaboration from Cabinet Office, Japan.

References

[1] Morris, A., and Madani, A., 1996. “Static and dynamic modelling of a two-flexible-link robot manipulator”. *Robotica,* **14**(3), p. 289–300.

[2] Lochan, K., Roy, B. K., and Subudhi, B., 2016. “A review on two-link flexible manipulators”. *Annual Reviews in Control,* **42**, pp. 346 – 367.

[3] Subudhi, B., and Morris, A., 2002. “Dynamic modelling, simulation and control of a manipulator with flexible links and joints”. *Robotics and Autonomous Systems,* **41**(4), pp. 257 – 270.

[4] Lotfazar, A., Eghtesad, M., Najafi, A., 2008. “Vibration Control and Trajectory Tracking for General In-Plane Motion of an Euler–Bernoulli Beam Via Two-Time Scale and Boundary Control Methods”. *ASME. J. Vib. Acoust.,* **130**(5):051009-051009-11. doi:10.1115/1.2948406.

[5] Lotfazar, A., Eghtesad, M., Najafi, A., 2009. “Exponential Stabilization of Transverse Vibration and Trajectory Tracking for General In-Plane Motion of an Euler–Bernoulli Beam Via Two-Time Scale and Boundary Control Methods”. *ASME. J. Vib. Acoust.,* **131**(5):054503-054503-7. doi:10.1115/1.3142888.

[6] Tso, S., Yang, T., Xu, W., and Sun, Z., 2003. “Vibration control for a flexible-link robot arm with deflection feedback”. *International Journal of Non-Linear Mechanics,* **38**(1), pp. 51 – 62.

[7] Njeri, W., Sasaki, M., and Matsushita, K., 2018. “Enhanced vibration control of a multilink flexible manipulator using filtered inverse controller”. *ROBOMECH Journal,* **5**(1), Nov, p. 28.

[8] Luo, Z. H., 1993. “Direct strain feedback control of flexible robot arms: new theoretical and experimental results”. *IEEE Transactions on Automatic Control,* **38**(11), Nov, pp. 1610–1622.

[9] Zhang, X., Xu, W., and Nair, S., 2004. “Comparison of some modeling and control issues for a flexible two link manipulator”. *ISA Transactions,* **43**(4), pp. 509 – 525.

[10] Hattori, M., Tadokoro, S., and Takamori, T., 1996. “A generalization of direct strain feedback control for a flexible structure with spatially varying parameters and a tip body”. *Transactions of the Institute of Systems, Control and Information Engineers,* **9**(12), pp. 606–608.

[11] Ge, S. S., Lee, T. H., and Zhu, G., 1998. “Improving regulation of a single-link flexible manipulator with strain feedback”. *IEEE Transactions on Robotics and Automation,* **14**(1), Feb, pp. 179–185.

[12] Lee, T., Ge, S., and Wang, Z., 2001. “Adaptive robust controller design for multi-link flexible robots”. *Mechatronics,* **11**(8), pp. 951 – 967.

[13] Luo, Z. H., and Sakawa, Y., 1993. “Gain adaptive direct strain feedback control of flexible robot arms”. In TENCON

Journal of Vibration and Acoustics. Received January 11, 2019;
Accepted manuscript posted March 13, 2019. doi:10.1115/1.4043241

'93. Proceedings. Computer, Communication, Control and Power Engineering.1993 IEEE Region 10 Conference on, Vol. 4, pp. 199–202 vol.4.

[14] Yang, S. M. , and Lee, G. S., 1997. "Vibration control of smart structures by using neural networks". *ASME. J. Dyn. Sys., Meas., Control.,* **119**(1): 34–39. doi:10.1115/1.2801211.

[15] Li, M., Wu, H., Wang, Y., Handroos, H., and Carbone, G., 2017. "Modified Levenberg–Marquardt Algorithm for Backpropagation Neural Network Training in Dynamic Model Identification of Mechanical Systems.". *ASME. J. Dyn. Sys., Meas., Control.,* **139**(3):031012-031012-14. doi:10.1115/1.4035010.

[16] Sasaki, M., Shimizu, T., Inoue, Y., and Book, W. J., 2012. "Self-tuning vibration control of a rotational flexible timoshenko arm using neural networks". *Advances in Acoustics and Vibration,* **2012**, pp. 1–7.

[17] Altay, A., Ozkan, O., and Kayakutlu G., 2019. "Prediction of aircraft failure times using artificial neural networks and genetic algorithms". *Journal of Aircraft,* **51**(1), Mar., pp. 47–53.

[18] Narendra, K. S., and Parthasarathy, K., 1991. "Gradient methods for the optimization of dynamical systems containing neural networks". *IEEE Transactions on Neural Networks,* **2**(2), March, pp. 252–262.

[19] Jafari. R., and Dhaouadi, R., 2011. "Adaptive pid control of a nonlinear servomechanism using recurrent neural networks". *Advances in Reinforcement Learning*, Jan., pp. 275–296.

[20] Mansour, T., Konno, A., and Uchiyama, M., 2012. "Neural network based tuning algorithm for MPID control". *PID Control, Implementation and Tuning*, Mansour, T., IntechOpen, doi: 10.5772/16058.

[21] Ripamonti, F., Orsini, L., and Resta, F., 2017. "A nonliear sliding surface in sliding mode control to reduce vibrations of a three-link flexible manipulator". *ASME. J. Vib. Acoust., 2017;* **139**(5):051005-051005-10. doi:10.1115/1.4036502.

[22] Karkoub, M., and Tamma, K., 2001. "Modelling and mu-synthesis control of flexible manipulators". *Computers & Structures,* **79**(5), pp. 543–551.

[23] Karkoub, M., Balas, G., Tamma, K., and Donath M., 2000. "Robust control of flexible manipulators via mu-synthesis". *Control Engineering Practice,* **8**(7), pp. 725–734.

[24] Bian, Y., Gao, Z., Lv, X., and Fan, M., 2018. "Theoretical and experimental study on vibration control of flexible manipulator based on internal resonance". *Journal of Vibration and Control,* **24**(15), pp. 3321–3337.

[25] Li, W., Luo, B., and Huang, H., 2016. "Active vibration control of flexible joint manipulator using input shaping and adaptive parameter auto disturbance rejection controller". *Journal of Sound and Vibration,* **363**, pp. 97–125.

[26] Liu, Z., Liu, J., and He, W., 2017. "Partial differential equation boundary control of a flexible manipulator with input saturation". *International Journal of Systems Science,* **48**(1), pp. 53–62.

Journal of Vibration and Acoustics. Received January 11, 2019;
Accepted manuscript posted March 13, 2019. doi:10.1115/1.4043241

[27] Nakamura, R., Sasaki, M., Takeuchi, T., and Ito, S., 2014. "Torsional vibration control of a flexible manipulator". *Journal of the Japan Society of Applied Electromagnetics and Mechanics,* **22**(2), pp. 261–267.

[28] Matsuno, F., and Endo, T., 2004. "Dynamics based control of two-link flexible arm". In The 8th IEEE International Workshop on Advanced Motion Control, 2004. AMC '04., pp. 135–140.

A Appendix

A.1 Manipulator specifications

[Table 1 goes here]

Journal of Vibration and Acoustics. Received January 11, 2019;
Accepted manuscript posted March 13, 2019. doi:10.1115/1.4043241

Table headings

Table 1. Specifications of the flexible manipulator system

Journal of Vibration and Acoustics. Received January 11, 2019;
Accepted manuscript posted March 13, 2019. doi:10.1115/1.4043241

Tables

Table 1: Specifications of the flexible manipulator system

Servomotor 1	Type	V850-012EL8	
Joint 1	Rated armature voltage	80	V
	Rated armature current	7.6	A
	Rated power	500	W
	Rated spindle speed	2500	rpm
	Rated torque	1.96	Nm
	Moment of inertia	6×10^{-4}	kgm^2
	Mass	4.0	Kg
Servomotor 2	Type	T511-012EL8	
Joint 2	Rated armature voltage	75	V
	Rated armature current	2	A
	Rated power	100	W
	Rated spindle speed	3000	rpm
	Rated torque	0.34	Nm
	Moment of inertia	3.7×10^{-5}	kgm^2
	Mass	0.95	Kg
Servomotor 3	Type	V404-012EL8	
Joint 3	Rated armature voltage	72	V
	Rated armature current	1	A
	Rated power	40	W
	Rated spindle speed	3000	rpm
	Rated torque	0.13	Nm
	Moment of inertia	8.4×10^{-6}	kgm^2
	Mass	0.4	Kg
Encoder	Reduction ratio	1/100	P/R
	Spring constant	1.6×10^4	Nm/rad

Journal of Vibration and Acoustics. Received January 11, 2019;
Accepted manuscript posted March 13, 2019. doi:10.1115/1.4043241

Harmonic drive	Type	CSF-40-100-2A-R-SP	
Joint 1	Reduction ratio	1/100	
	Spring constant	23	Nm/rad
	Moment of inertia	4.50×10^{-4}	kgm^2
Harmonic drive	Type	CSF-17-100-2A-R-SP	
Joint 2	Reduction ratio	1/100	
	Spring constant	1.6×10^{-4}	Nm/rad
	Moment of inertia	7.9×10^{-6}	kgm^2
Harmonic drive	Type	CSF-14-100-2A-R-SP	
Joint 3	Reduction ratio	1/100	
	Spring constant	7.1×10^{-5}	Nm/rad
	Moment of inertia	3.3×10^{-6}	kgm^2
Link1	Material	Stainless steel	
	Length	0.44	m
	Radius	5×10^{-3}	m
Link2	Material	Aluminum	
	Length	0.44	m
	Radius	4×10^{-3}	m
Strain Gauge	Type	KGF-2-120-C1-23L1M2R	

Journal of Vibration and Acoustics. Received January 11, 2019;
Accepted manuscript posted March 13, 2019. doi:10.1115/1.4043241

List of Figures

Fig. 1. Control setup of the flexible manipulator

Fig. 2. DC servomotor model

Fig. 3. 3D, two-link flexible manipulator

Fig. 4. Bending moments due to the self-weight of the links

Fig. 5. Multilayer neural network configuration

Fig. 6. Self-tuning strain feedback gain system configuration

Fig. 7. Simulations of control law, strain and feedback gains before modification (a) Control law (b) Link strain (c) Feedback gains

Fig. 8. Simulations of control law, strain and feedback gains after modification (a) Control law (b) Link strain (c) Feedback gains

Fig. 9. Simulations of strain, with and without strain feedback (a) Link 1 torsion (b) Link 1 in-plane (c) Link 2 in-plane

Fig. 10. Link strain without any load (a) Link 1 torsion (b) Link 1 in-plane (c) Link 2 in-plane

Fig. 11. Joint trajectories without any load (a) Joint 1 (b) Joint 2 (c) Joint 3

Fig. 12. Feedback gains without any load (a) Link 1 torsion (b) Link 1 in-plane (c) Link 2 in-plane

Fig. 13. Strain power spectrum without any load (a) Link 1 torsion (b) Link 1 in-plane (c) Link 2 in-plane

Fig. 14. Link strain with a load of 100g (a) Link 1 torsion (b) Link 1 in-plane (c) Link 2 in-plane

Fig. 15. Joint trajectories with a load of 100g (a) Joint 1 (b) Joint 2 (c) Joint 3

Fig. 16. Feedback gains with a load of 100g (a) Link 1 torsion (b) Link 1 in-plane (c) Link 2 in-plane

Fig. 17. Strain power spectrum with a load of 100g (a) Link 1 torsion (b) Link 1 in-plane (c) Link 2 in-plane

Figures

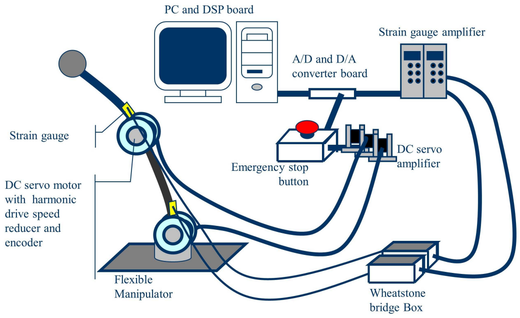

Fig. 1: Control setup of the flexible manipulator

Journal of Vibration and Acoustics. Received January 11, 2019;
Accepted manuscript posted March 13, 2019. doi:10.1115/1.4043241

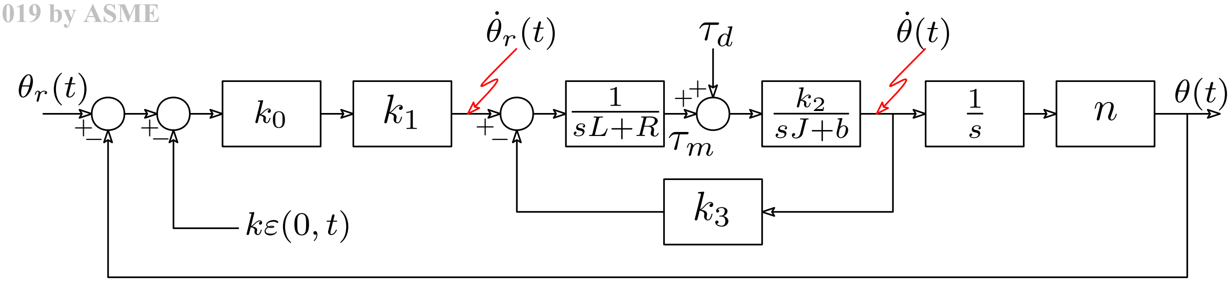

Fig. 2: DC servomotor model

Journal of Vibration and Acoustics. Received January 11, 2019;
Accepted manuscript posted March 13, 2019. doi:10.1115/1.4043241

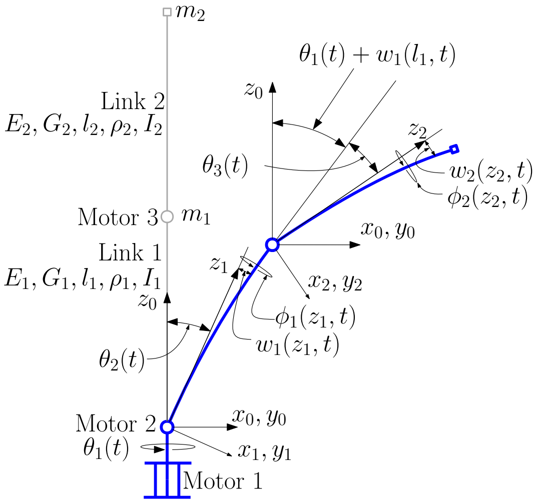

Fig. 3: 3D, two-link flexible manipulator

Journal of Vibration and Acoustics. Received January 11, 2019;
Accepted manuscript posted March 13, 2019. doi:10.1115/1.4043241

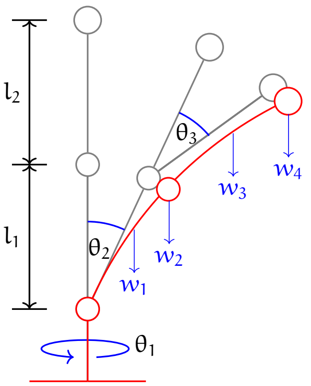

Fig. 4: Bending moments due to the self-weight of the links

Journal of Vibration and Acoustics. Received January 11, 2019;
Accepted manuscript posted March 13, 2019. doi:10.1115/1.4043241

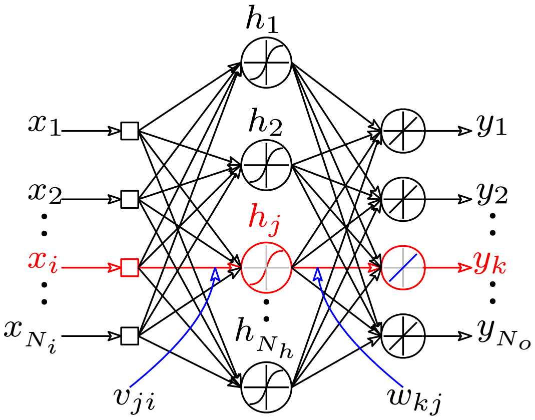

Fig. 5: Multilayer neural network configuration

Journal of Vibration and Acoustics. Received January 11, 2019;
Accepted manuscript posted March 13, 2019. doi:10.1115/1.4043241

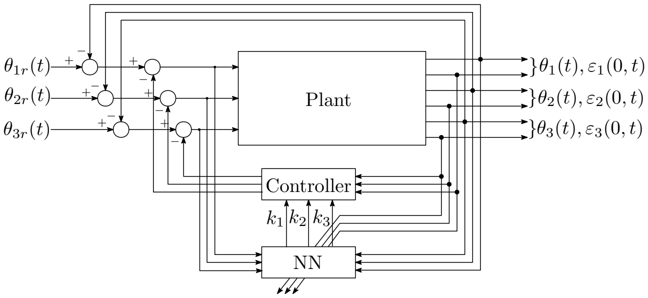
$\theta_{1r}(t)$
$\theta_{2r}(t)$
$\theta_{3r}(t)$
+
−
Plant
$\}\theta_1(t), \varepsilon_1(0,t)$
$\}\theta_2(t), \varepsilon_2(0,t)$
$\}\theta_3(t), \varepsilon_3(0,t)$
Controller
k_1
k_2
k_3
NN

Fig. 6: Self tuning strain feedback gain system configuration

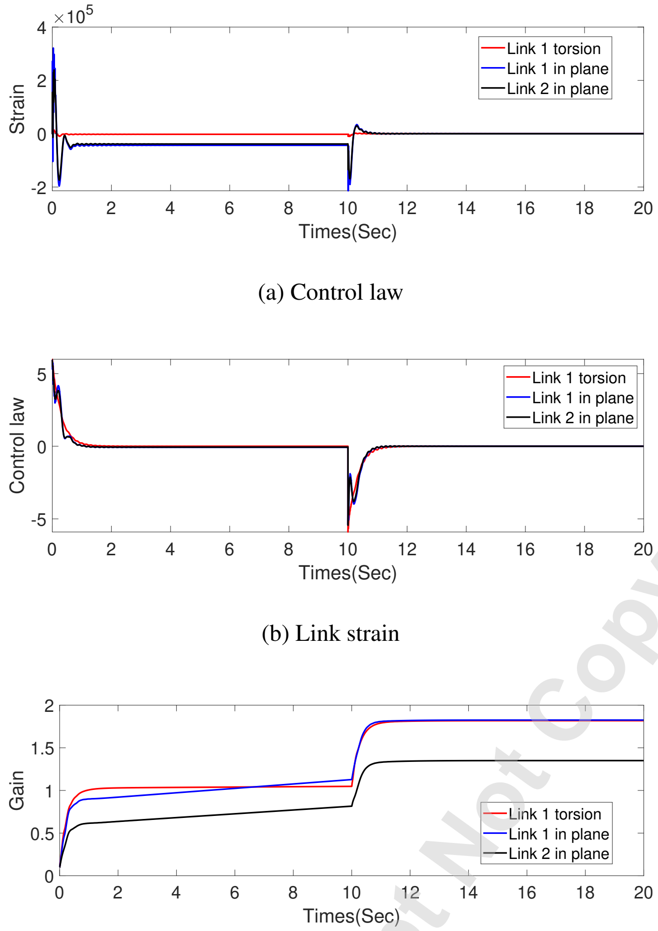

(a) Control law

(b) Link strain

(c) Feedback gains

Fig. 7: Simulations of control law, strain and feedback gains before modification

Journal of Vibration and Acoustics. Received January 11, 2019;
Accepted manuscript posted March 13, 2019. doi:10.1115/1.4043241
Copyright © 2019 by ASME

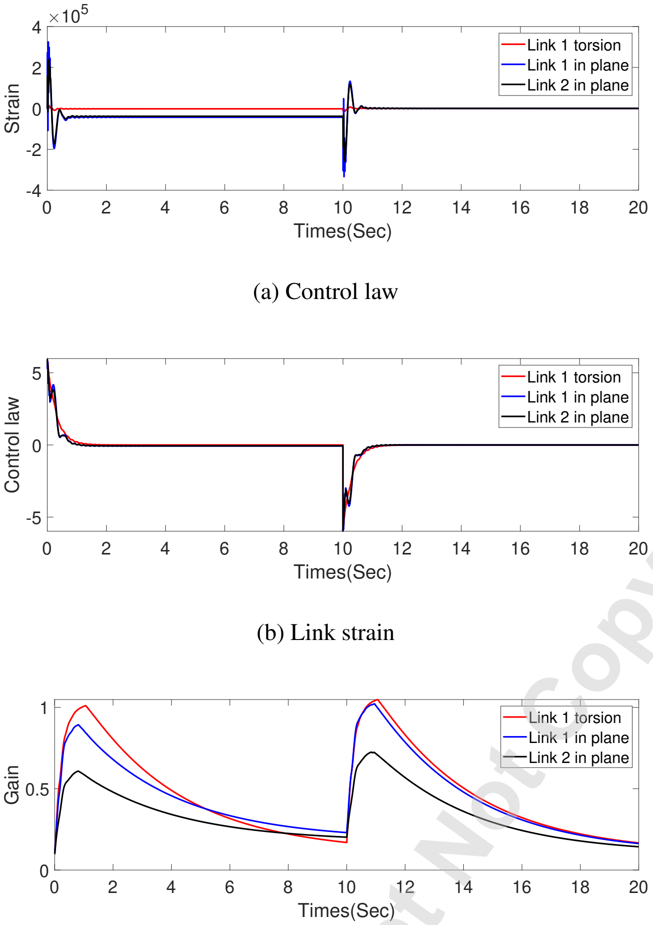

(a) Control law

(b) Link strain

(c) Feedback gains

Fig. 8: Simulations of control law, strain and feedback gains after modification

Journal of Vibration and Acoustics. Received January 11, 2019;
Accepted manuscript posted March 13, 2019. doi:10.1115/1.4043241

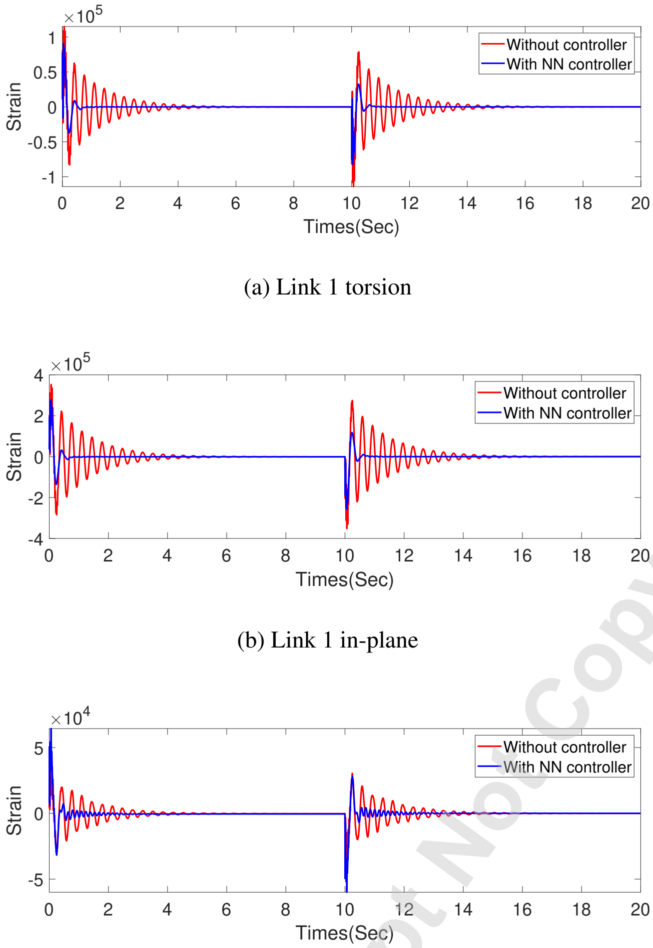

(a) Link 1 torsion

(b) Link 1 in-plane

(c) Link 2 in-plane

Fig. 9: Simulations of strain, with and without strain feedback

Journal of Vibration and Acoustics. Received January 11, 2019;
Accepted manuscript posted March 13, 2019. doi:10.1115/1.4043241

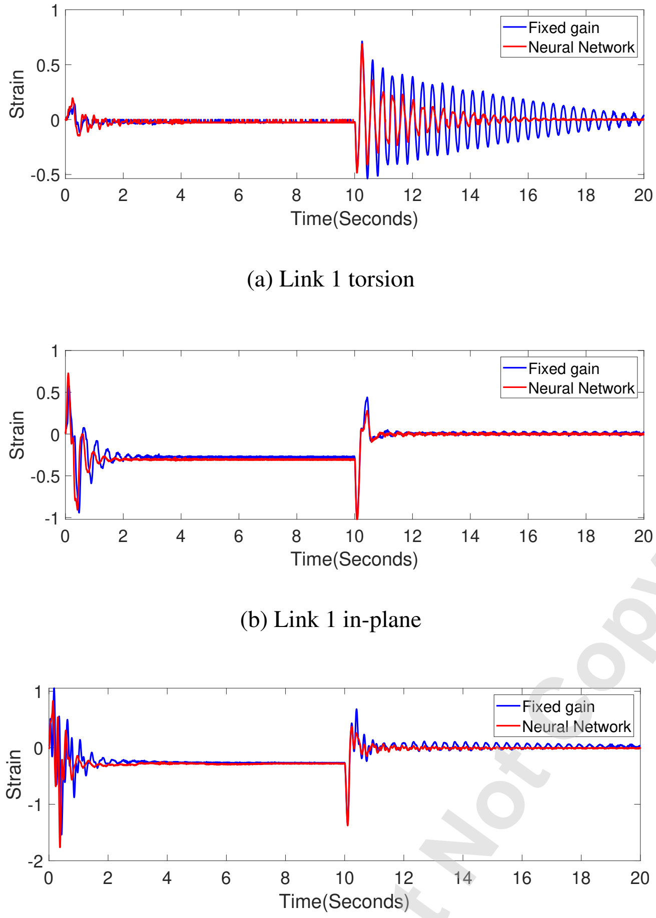

(a) Link 1 torsion

(b) Link 1 in-plane

(c) Link 2 in-plane

Fig. 10: Link strain without any load

Journal of Vibration and Acoustics. Received January 11, 2019;
Accepted manuscript posted March 13, 2019. doi:10.1115/1.4043241
Copyright © 2019 by ASME

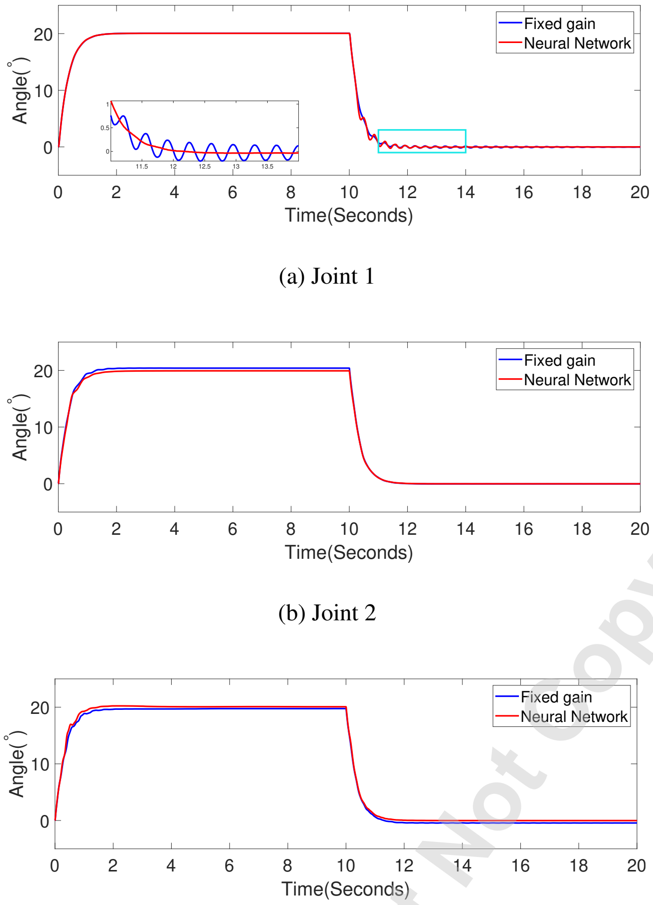

(a) Joint 1

(b) Joint 2

(c) Joint 3

Fig. 11: Joint trajectories without any load

Journal of Vibration and Acoustics. Received January 11, 2019;
Accepted manuscript posted March 13, 2019. doi:10.1115/1.4043241

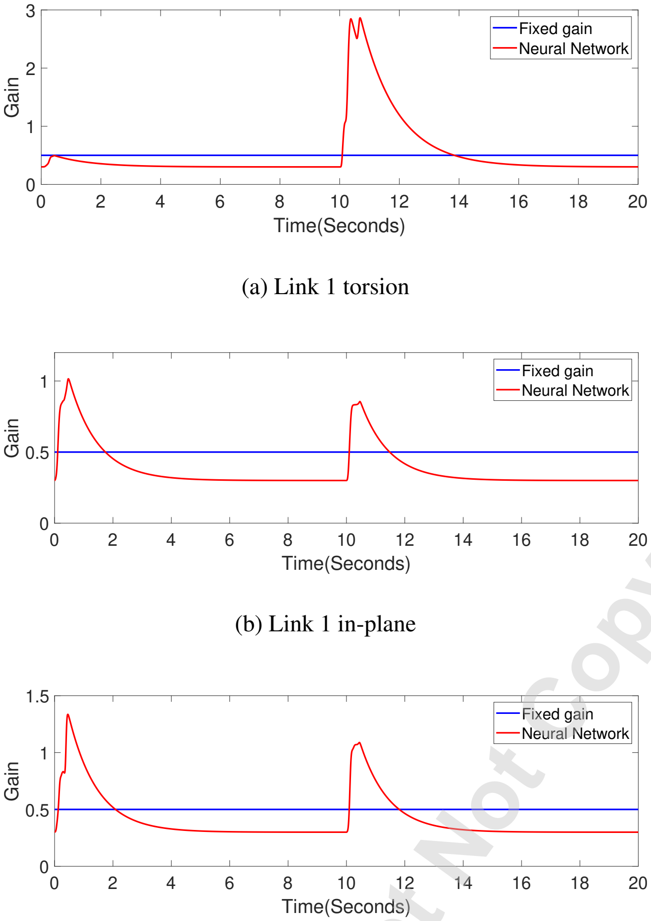

(a) Link 1 torsion

(b) Link 1 in-plane

(c) Link 2 in-plane

Fig. 12: Feedback gains without any load

Journal of Vibration and Acoustics. Received January 11, 2019;
Accepted manuscript posted March 13, 2019. doi:10.1115/1.4043241

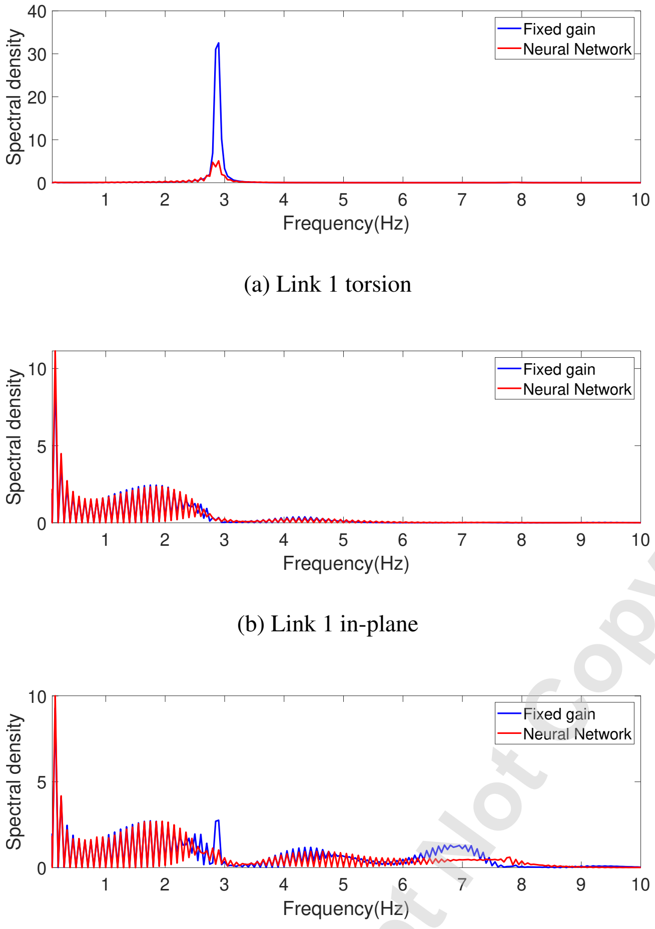

(a) Link 1 torsion

(b) Link 1 in-plane

(c) Link 2 in-plane

Fig. 13: Strain power spectrum without any load

Journal of Vibration and Acoustics. Received January 11, 2019;
Accepted manuscript posted March 13, 2019. doi:10.1115/1.4043241

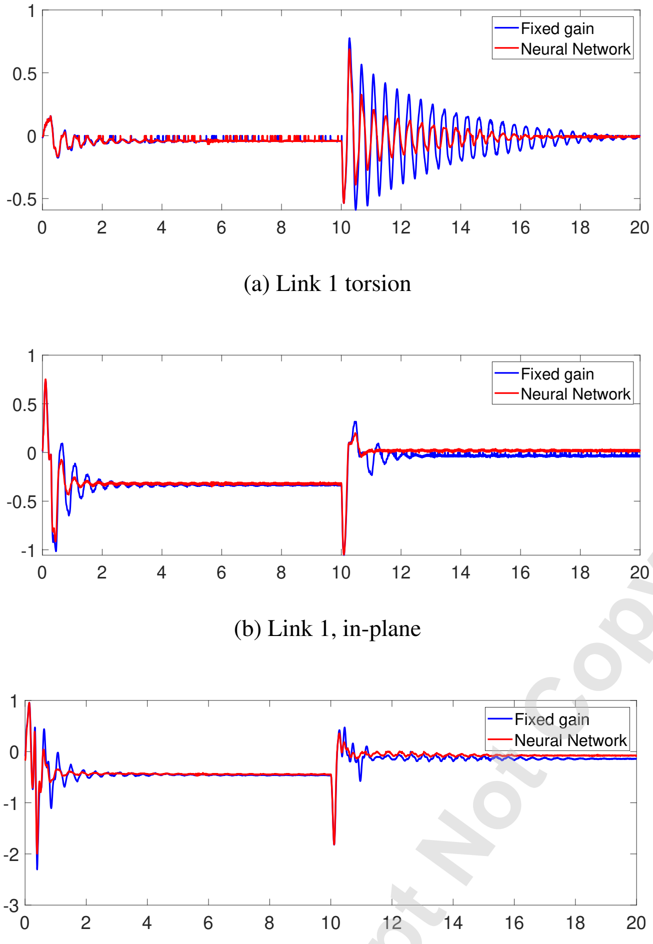

(a) Link 1 torsion

(b) Link 1, in-plane

(c) Link 2, in-plane

Fig. 14: Link strain with a load of 100g

Journal of Vibration and Acoustics. Received January 11, 2019;
Accepted manuscript posted March 13, 2019. doi:10.1115/1.4043241

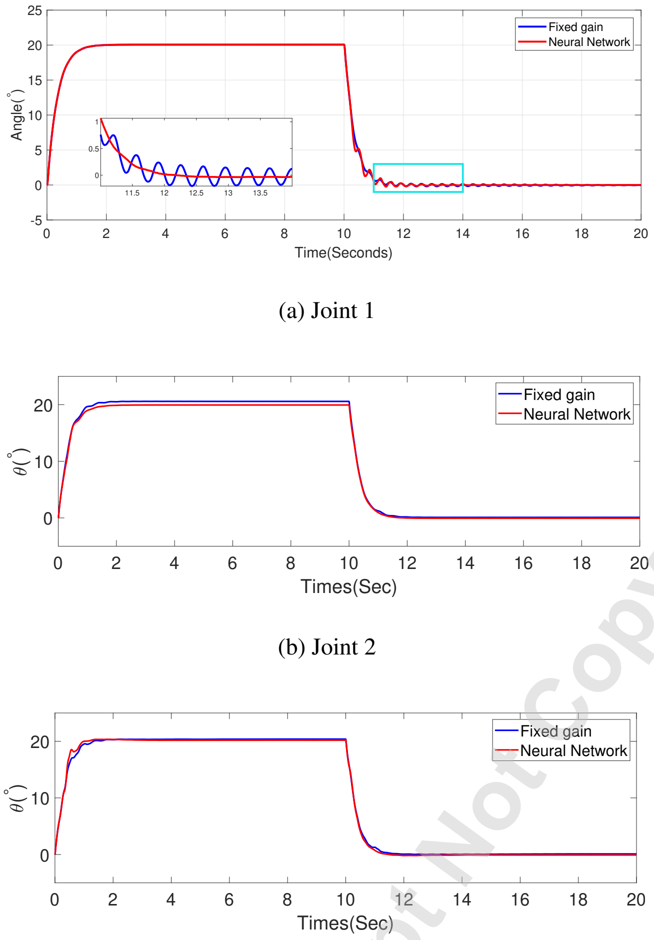

(a) Joint 1

(b) Joint 2

(c) Joint 3

Fig. 15: Joint trajectories with a load of 100g

Journal of Vibration and Acoustics. Received January 11, 2019;
Accepted manuscript posted March 13, 2019. doi:10.1115/1.4043241

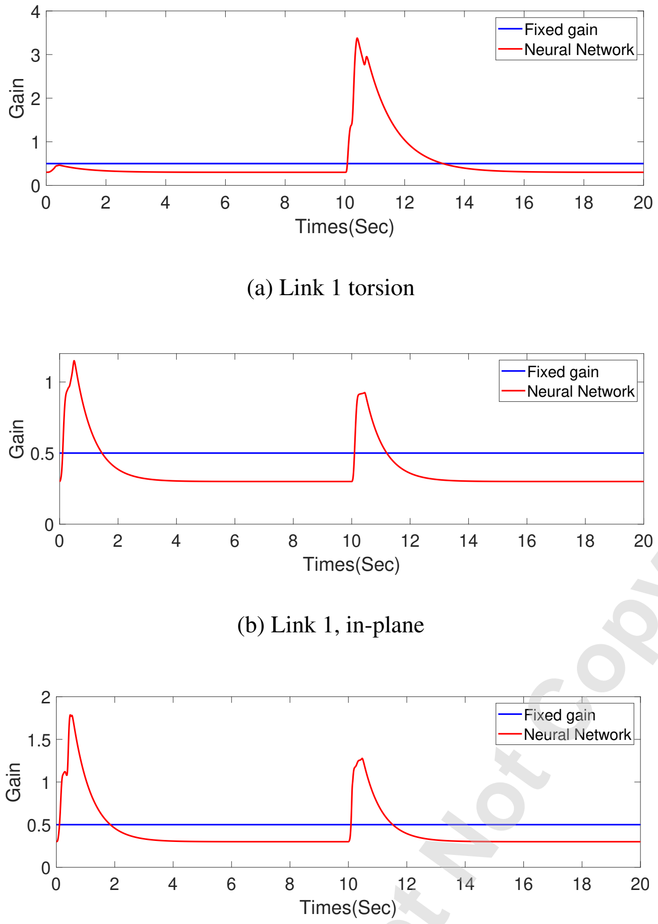

(a) Link 1 torsion

(b) Link 1, in-plane

(c) Link 2, in-plane

Fig. 16: Feedback gains with a load of 100g

Journal of Vibration and Acoustics. Received January 11, 2019;
Accepted manuscript posted March 13, 2019. doi:10.1115/1.4043241
Copyright © 2019 by ASME

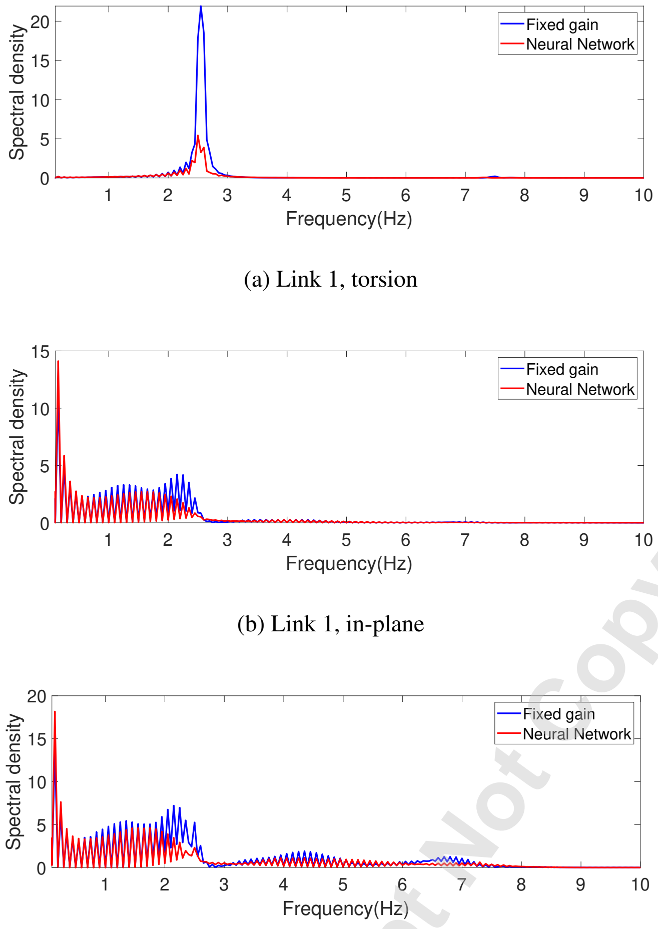

(a) Link 1, torsion

(b) Link 1, in-plane

(c) Link 2, in-plane

Fig. 17: Strain power spectrum with a load of 100g